Supplementary Information

NIR-II fluorescent imaging without intended excitation light

Aiyan Ji‡,[ab] Hongyue Lou‡,[b] Jiafeng Li,[b] Yimeng Hao,[a] Xiaonan Wei,[b] Yibin Wu,[b] Weili Zhao*,[a] Hao Chen*[bcd], Zhen Cheng*[abde]

a. Department of Pharmacy, School of Pharmacy, Fudan University, Shanghai, 201203, China;

b. State Key Laboratory of Drug Research, Molecular Imaging Center, Shanghai Institute of Materia Medica, Chinese Academy of Sciences, Shanghai, 201203, China;

c. State Key Laboratory of Chemical Biology, Shanghai Institute of Materia Medica, Chinese Academy of Sciences, Shanghai, 201203, China;

d. Shandong Laboratory of Yantai Drug Discovery, Bohai rim Advanced Research Institute for Drug Discovery, Yantai, Shandong 264117, China;

e. University of Chinese Academy of Sciences, No.19A Yuquan Road, Beijing 100049, China.

‡ These authors contributed equally to this work.

General materials and instruments

UV–vis-NIR absorption spectroscopy were performed on SHIMADZU UV-2600 spectrophotometer (Shimadzu Common Container (Version 2.70)). Fluorescence emission spectroscopy were performed on iHR320-imaging-spectrometer. The reflection spectrum of different light sources were performed on FX2000 fiber spectrometer (Ideaoptics, China). The data were finally recorded on the computer equipped to the spectrometer (Morpho3.2). Deionized water was obtained from a Millipore Milli-DI water purification system (Merck). MTT (3-(4,5- dimethylthiazol-2-yl)- 2,5-diphenyl tetrazolium bromide) assay kits were purchased from Dalian Meilun Biotechnology Co., Ltd. The hydrodynamic diameter was measured by dynamic light scattering (DLS) on a Zatesizer (Nano-ZS, Malvern instruments, UK). Transmission electron microscope (TEM) images were obtained on a JEOL JEM-2100 electron microscope (accelerating voltage: 120 KV). The NIR-II fluorescence images were collected by *vivo* imaging system, which is equipped with a water-cooled InGaAs SWIR camera (NIRvana-640, Teledyne Princeton Instruments, 640 × 512 pixel). The zoom-stereo microscope equipped with a fixed 1× lens and 0.64 × -4.50 × zoom lens was also used for large field of view. Power measurement of different light sources through standard photodiode power sensor (S121C, 400-1100 nm, 500 mW, Thorlabs) or thermal power sensor head, surface absorber (S425C-L, 0.19 - 20 μm, 50 W, Thorlabs). The fluorescence was then detected by a liquid-nitrogen-cooled InGaAs camera (NIRvana 640, Teledyne Princeton Instruments). All images were background corrected in the Light Field imaging software (Version 6.11.4) and processed with image *J* (Version1.8.0). Origin (Version 9.6) was used to analyze the spectrum images. All statistical analyses were performed by Graphpad Prism (Version 8.0.2). Adobe Illustrator CC 2018 (Version 22.1.0) was used to edit the images.

Methods

Density functional theory calculations for TPA-TQT. Density function theory calculation was performed on time dependent density functional theory (TD-DFT) calculations at B3LYP/6-31G (d, p) level (Gaussian 03), solvent = dichloromethane. To reduce the computational requirements, dialkyl chains were replaced by methyl. $\Delta E = E_{LUMO}-E_{HOMO}$.

The chemical stability of ICG and TPA-TQT. To test the chemical stability of ICG and TPA-TQT, we performed co-incubation experiments with dyes and Reactive Oxygen/Nitrogen Species (ROS/RNS). Briefly, Nitrite (NO_2^-) was prepared by dissolving sodium nitrite in deionized water. Hypochloride anion (ClO^-) was prepared by NaClO. H_2O_2 solution (10 mM) was provided by diluting 30% H_2O_2. The single oxygen ($^1O_2$) was produced by the reaction between NaClO (10 mM) and H_2O_2 (10 mM). ICG and TPA-TQT (10 μM) were incubated with these active molecules (1 mM) in a 37^0C water bath for 30 min. Then, the absorption spectra of ICG and TPA-TQT were measured.

Photostability. ICG and TPA-TQT aqueous solution or TPA-TQT in serum were exposed to 808 nm laser (145 mW cm^{-2}) or X-Cite® 110LED （45 mW cm^{-2}） for 30 minutes. The fluorescence intensities were recorded by an InGaAs SWIR camera during duration.

Preparation of TPA-TQT protein complexes. Prepared 1 mM TPA-TQT, 100 μM HSA/BSA in 1 × phosphate buffered saline (PBS) solution. Added 10 μL of 1 mM TPA-TQT into 200 uL of 100 μM HSA/BSA solution to keep the molar ratio of TPA-TQT: HSA/BSA at 1:2. For fetal bovine serum (FBS), 10 μL of 1 mM TPA-TQT was added into 200 μL of 20% FBS. For TPA-TQT heated complexes, the dye–protein complexes were added in a sealed microcentrifuge tube and incubated into 70-75℃ water baths for 15 min. All samples were detected under X-Cite® 110LED excitation, 1000 nm long-pass filter. In the following imaging experiments, the dye-protein

complexes were used right after preparation. The fluorescence brightness of TPA-TQT/protein heated to 70°C was termed as TPA-TQT@protein-H (TPA-TQT@BSA-H, TPA-TQT@HSA-H, and TPA-TQT@FBS-H).

Preparation of TPA-TQT-TMS NPs. Briefly, TPA-TQT-TMS (1 mg) and DSPE-PEG_{2000} (5 mg) were dissolved in tetrahydrofuran (THF) (0.5 mL) and the mixed solution was stirred vigorously at room temperature for 0.5 h. After the mixture was added into Milli-Q water (20 mL), the solution was sonicated with a Microtip sonicator at 45 W output power for 2 min. The obtained mixture was stirred vigorously to evaporate THF at room temperature. Then, the final solution was filtered and concentrated with a 30 K ultrafiltration tube. The filtrate was washed with deionized water for 3 times, and it was concentrated and purified to obtain TPA-TQT-TMS NPs.

Quantum yield of TPA-TQT-TMS NPs. The quantum yield of TPA-TQT-TMS NPs in water was determined by using the dye IR-26 (QY_{ref} = 0.05% in 1,2-dichloroehane (DCE) as reference). The quantum yield was calculated in the following manner:

$$QY_{sample} = QY_{ref} \times \frac{n_{sample}^{2}}{n_{ref}^{2}} \times \frac{Slope_{sample}}{Slope_{ref}}$$

Where QY_{ref} is the quantum yield of IR-26 in dichloroethane; n_{ref} and n_{sample} are the refractive indices of IR-26 and TPA-TQT-TMS NPs in DCE (1,.444) and water (1.333). The $Slope_{sample}$ (TPA-TQT-TMS NPs) and $Slope_{ref}$ (IR-26) are the slopes obtained by linear fitting of the integrated emission spectra and the OD value at 808 nm.

Cell culture. U87MG (human glioma cell), 4T1 (mouse breast cancer cells) and 3T3 (mouse embryonic fibroblast cell) were cultured in DMEM containing high glucose (Gibco), which were supplemented with 10% FBS and 1% penicillin-streptomycin. The cells were expanded in a tissue culture dish and maintained in a humid atmosphere of 5% CO_2 at 37°C. The culture medium was changed every other day. The 0.5% trypsin was used to detach the cells and dissociated into a single cell suspension for inoculation.

Cytotoxicity of TPA-TQT. Cell toxicity of NIH-3T3 cells treated with TPA-TQT at different concentrations ranging from 0 to 200 μM for 24 h. Murine fibroblast 3T3 cells were plated into a 96 well plate at a concentration of 1×10^4 cells/well in DMEM with 10% FBS at 37°C and 5% CO_2, and 24 h later, the cells were incubated with TPA-TQT with different concentrations (200 μM, 100 μM, 50 μM, 0 μM) for 24 h. Then 20 μL of the 5 mg/mL MTT stock solution was added and incubated for 4 hours. After removing medium, 150 μL DMSO was added to dissolve the formazan crystals precipitates. After shaking the cell plate for 5 min, the absorbance (A) at a wavelength of 490 nm was measured with a Tecan microplate reader (SoftMax Pro 7.1.lnk (Version 7.1.1)). Data are presented as mean ± s.d. derived from n = 4 independent measurements.

Animal studies. All the following animal procedures were approved by the Shanghai Experimental Animal Center of Chinese Academy of Sciences guidelines and performed under the institutional guidelines for animal handling. All operations related to animal experiments follow the relevant requirements of the Institutional Animal Care and Use Committee (IACUC) of Shanghai Institute of Material Medica, Chinese Academy of Sciences. All Mice were housed under specific pathogen free (SPF) conditions. The feeding environment was 25°C, with a humidity of 35-45%, alternating light and dark for 12 hours. All animals were kept free to drink and eat.

For subcutaneous U87MG inoculation, 5×10^6 U87MG cells were injected into the subcutaneous tissue of the right buttocks of 6-week-old nude mice. Imaging experiments were performed when the tumor diameter reached around 4 mm. Subcutaneous and metastatic 4T1 tumor model was established as following. Specifically, 6-week-old Balb/c mice were depilated before model establishment. 1×10^6 4T1 cells were injected into the subcutaneous tissue of the right buttocks or the right shoulder of mice. As the subcutaneous tumor grew, the tumor metastasized to the liver and intestine for colonization. Imaging experiments were performed when the subcutaneous 4T1 tumor diameter reached around 1 cm. During the *in vivo* NIR-II

imaging, the mice were kept anesthetized by a nose cone delivering air mixed with 4% isoflurane. Mice were randomly selected for all experiments. The injected dose was a 200 μL in a 1 × PBS (pH = 7.4) solution at a specified concentration. Metastatic 4T1 tumor model was the remote metastasis of subcutaneous tumor.

Multi-wavelength LED-based NIR-II vascular imaging. Six-week-old Balb/c mice (n = 3 per group) were depilated all hair before imaging. TPA-TQT@BSA-H or ICG@BSA (65 nM, the molar ratio of dye: BSA at 1:2) were injected intravenously, and fluorescence images were collected at different time points (20 s, 15 min, 30 min, 60 min) after injection under X-Cite® 110LED, 660 nm and 808 nm laser excitation with 1000 nm, 1100 nm, 1200 nm, 1300 nm long-pass filters.

Multi-wavelength LED-based NIR-II imaging of lymphatic drainage and lymphatic inflammation. Lipopolysaccharide (LPS) induced lymphatic inflammation model: six-week-old Balb/c mice (n = 3 per group) were anaesthetized using rodent ventilator with air mixed with 4% isoflurane and were depilated hair on the hindlimb. LPS (93 $\mu g \cdot \mu L^{-1}$, 10 μL) and PBS (10 μL) were injected subcutaneously into the hindlimb pads of mice. After injection of LPS and PBS for 4 hours, TPA-TQT@BSA-H (50 μg) or ICG (24 μg) were injected subcutaneously into the hindlimb pads, or TPA-TQT@BSA-H (200 ug) via intravenous administration. Then, fluorescence images were collected under X-Cite® 110LED excitation.

Multi-wavelength-LED based NIR-II imaging of hindlimb ischemic reperfusion. Six-week-old Balb/c mice (n = 6) were anaesthetized using rodent ventilator with air mixed with 4% isoflurane and were depilated hair on the hind legs. Along the vessels in the left hindlimb, the skin was cut, and the vessels and muscle tissue were bluntly dissected. Finally, the left vein and femoral artery were ligated with a hemostat following the protocol reported previously. TPA-TQT@BSA-H (5 $mg \cdot kg^{-1}$) was intravenous injected into mice at 30 min after ligation, and the hemostat were removed simultaneously. The process of the ischemic reperfusion in hindlimbs was recorded.

Fluorescent signal intensities at the proximal and distal of the left vein and femoral artery ligation site were used to evaluate the progression of ischemia-reperfusion.

NIR-II imaging of tumor vascular and image-guided surgery excited by LED light source. For assessing blood vessels in the U87MG tumor, nude mice bearing subcutaneous U87MG glioma (n = 3 per group) were imaged after injection with TPA-TQT-TMS NPs (366 μg, 200 μL). Emission was typically collected with 1000, 1200, 1300 nm LP filter under the excitation of multi-wavelength LED light source.

Subcutaneous 4T1 tumor metastasized in liver and intestinal (n = 3) were resected post intravenous injection of TPA-TQT-TMS NPs (9 $mg \cdot kg^{-1}$) under NIR-II fluorescent bioimaging guidance with multi-wavelength (X-cite® 110LED) and broadband (lighting LED) LED light excitation. Under the guidance of fluorescent signals by LED light, the abdominal skin and peritoneum were opened, and then the tissues with prominent fluorescent signals in the liver and intestinal were removed. All collected tissues were analyzed by H&E staining.

Statistical analysis.

All data acquired in this study were presented as the mean ± s.d. Differences between groups were assessed using unpaired two-tailed Student's t tests for two groups. $*P < 0.05$ was considered statistically significant.

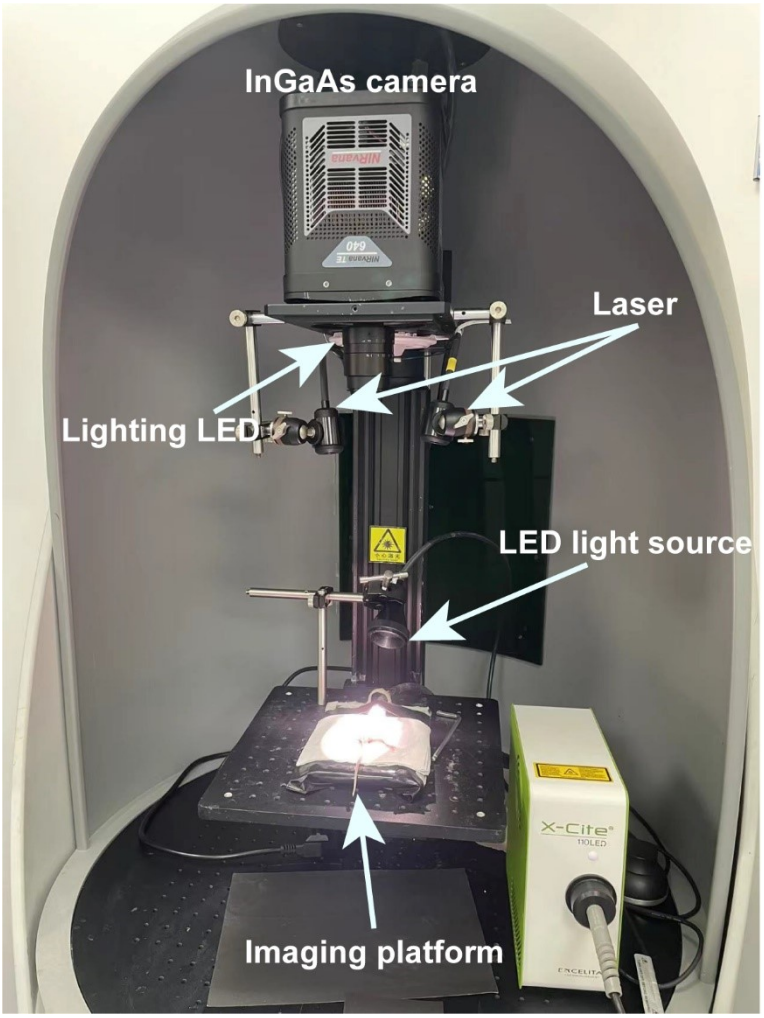

Supplementary Figure 1. Photograph of multi-wavelength LED-based NIR-II fluorescent imaging setup.

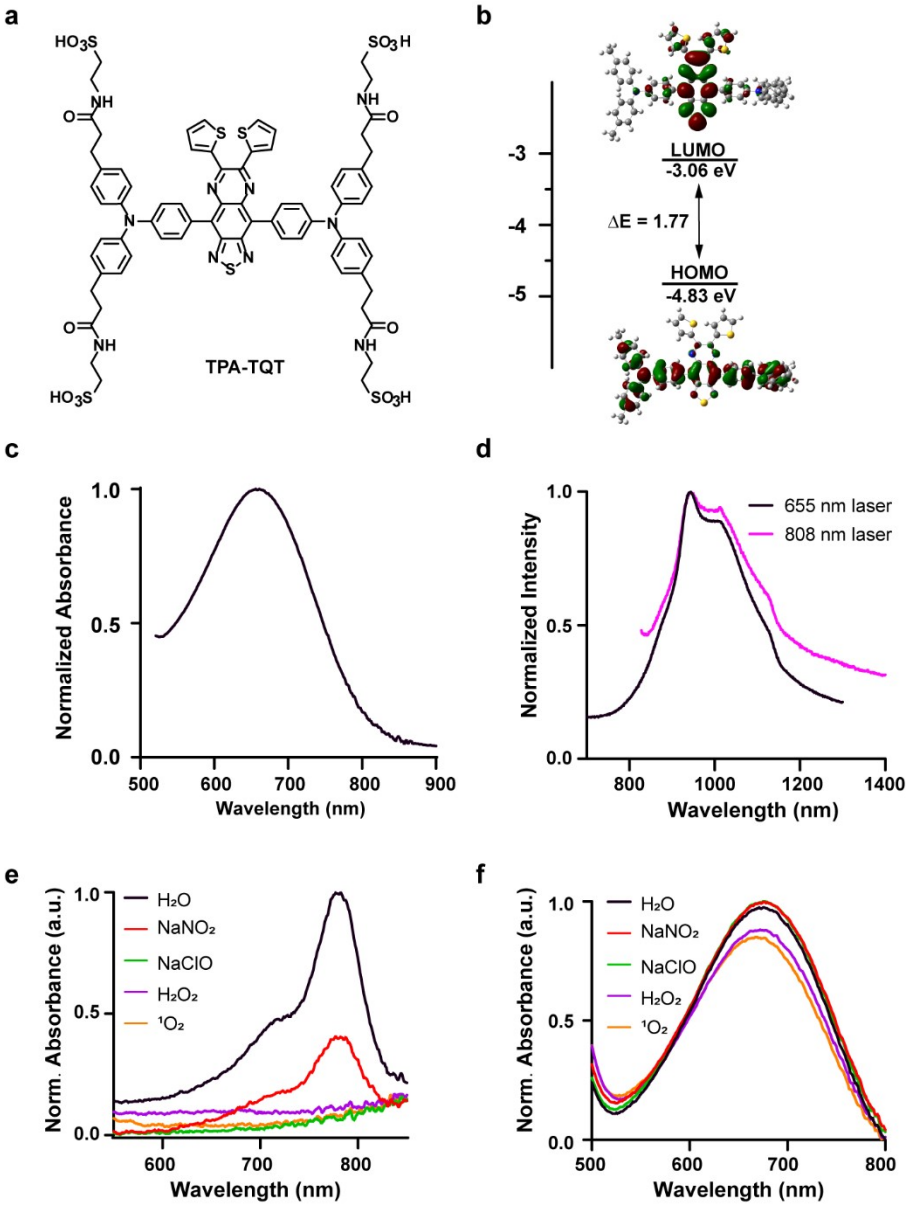

Supplementary Figure 2. Photo-physical characterization of TPA-TQT. **a)** Chemical structure of TPA-TQT. **b)** Highest occupied molecular orbital (HOMO) and lowest unoccupied molecular orbitals (LUMO) of TPA-TQT using Gaussian 09 time dependent density functional theory (TD-DFT) calculations at B3LYP/6-31G (d, p) level; solvent = dichloromethane. To reduce the computational requirements, dialkyl chains were replaced by methyl. **c)** Absorption spectrum of TPA-TQT in deionized water. **d)** The fluorescence emission spectrum of TPA-TQT in deionized water excited by 655 nm and 808 nm laser. **e, f**) Changes of absorption curves of ICG (**e**) and TPA-TQT (**f**) after reaction with different reactive oxygen/nitrogen species (ROS/RNS).

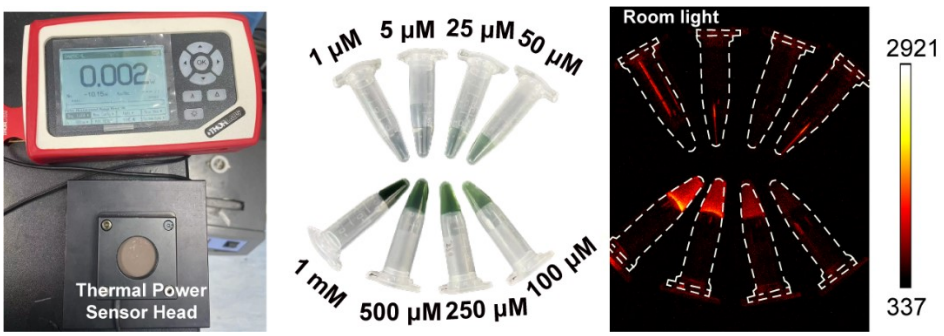

Supplementary Figure 3. TPA-TQT NIR-II imaging excited by LED room light without other excitation light sources. (1000 nm LP, 1000 ms, 0.35 mW cm^{-2}).

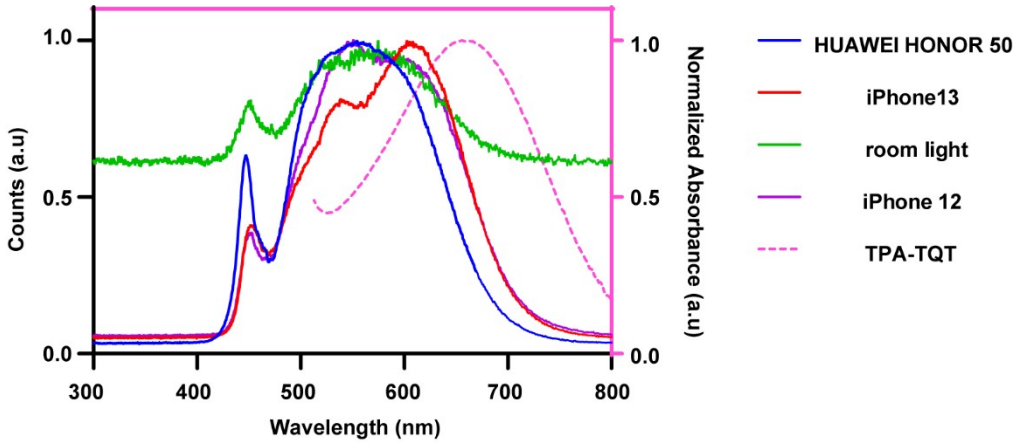

Supplementary Figure 4. Absorbance spectra of TPA-TQT and spectra of different light sources, including HUAWEI HONOR 50, iPhone 12/13, and LED room light.

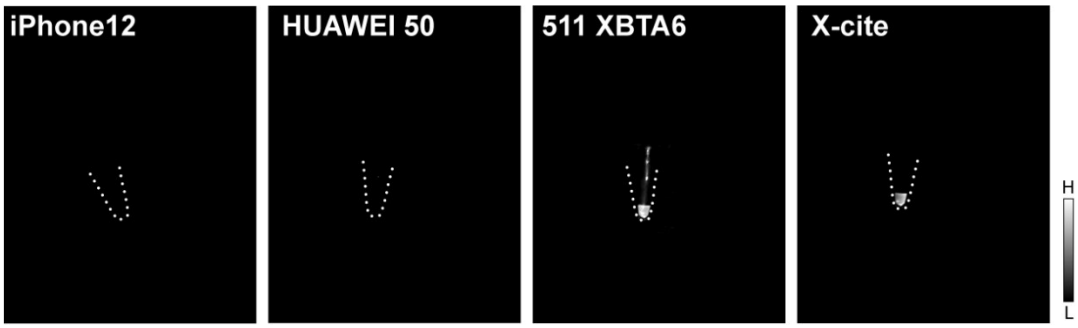

Supplementary Figure 5. *In vitro* NIR-II fluorescent images of TPA-TQT (5 μg/μL) in deionized water excited by different LED light sources, including iPhone 12, HUAWEI 50, 5.11 XBT A6 flashlight and X-Cite® 110LED (1000 nm LP, 200 ms).

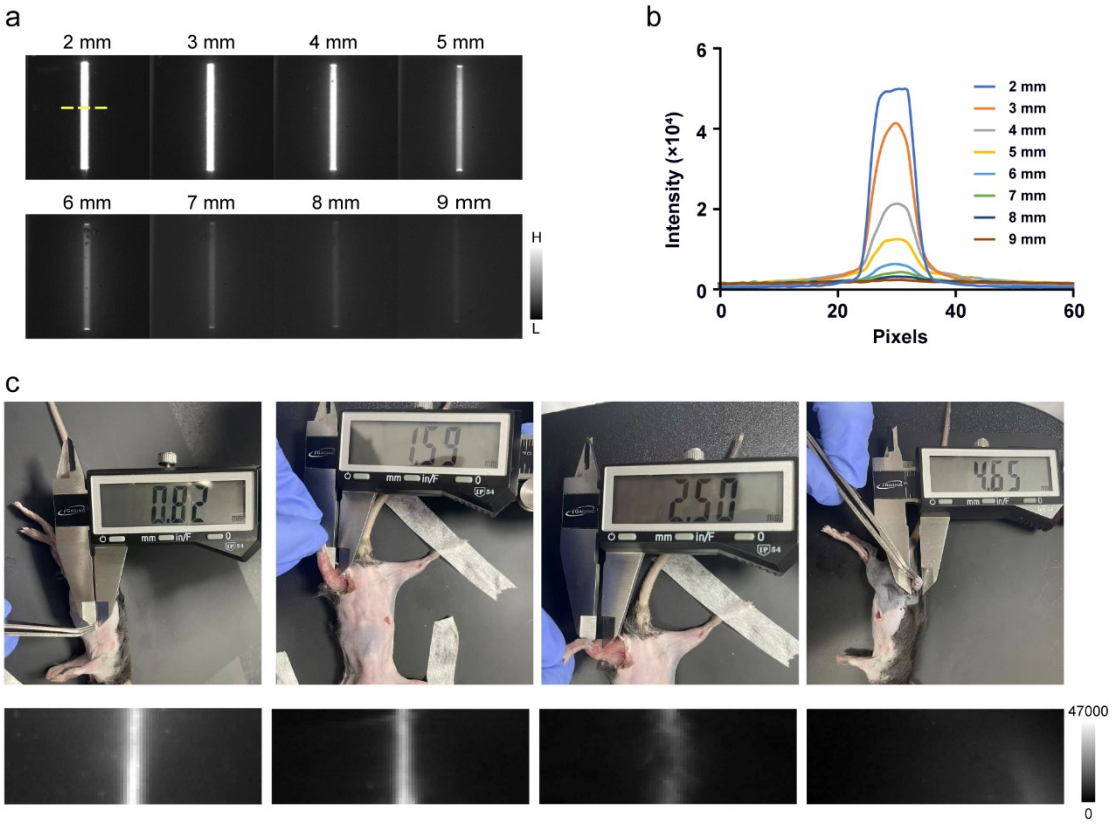

Supplementary Figure 6. Multi-wavelength LED excited NIR-II imaging for evaluation of tissue penetration. **a)** NIR-II Fluorescence images of capillaries filled with TPA-TQT, immersed in 1% intralipid with varying depth (X-cite® 110LED, 1000 nm LP, 200 ms). **b)** NIR-II fluorescence intensity profiles of capillaries filled with TPA-TQT across the yellow dotted lines at different immersion depths in 1% intralipid. **c)** NIR-II fluorescence images of capillaries filled with TPA-TQT, immersed in mouse tissues at different depths, including shin, muscle and tumor. (X-cite® 110LED, 1000 nm LP, 500 ms).

Supplementary Figure 7. **a)**. Cell toxicity of NIH-3T3 cells treated with TPA-TQT at different concentrations ranging from 0 to 200 μM for 24 h. **b)**. NIR-II stereo microscopy imaging of TPA-TQT (100 μM) with 808 nm laser and white LED as excitation light in 4T1 cells. Scale bar: 100 μm. (808 nm laser, 140 mW cm^{-2}, 1000 LP, 2000 ms) (X-cite® 110LED, 45 mW cm^{-2}, 1000 LP, 5000 ms).

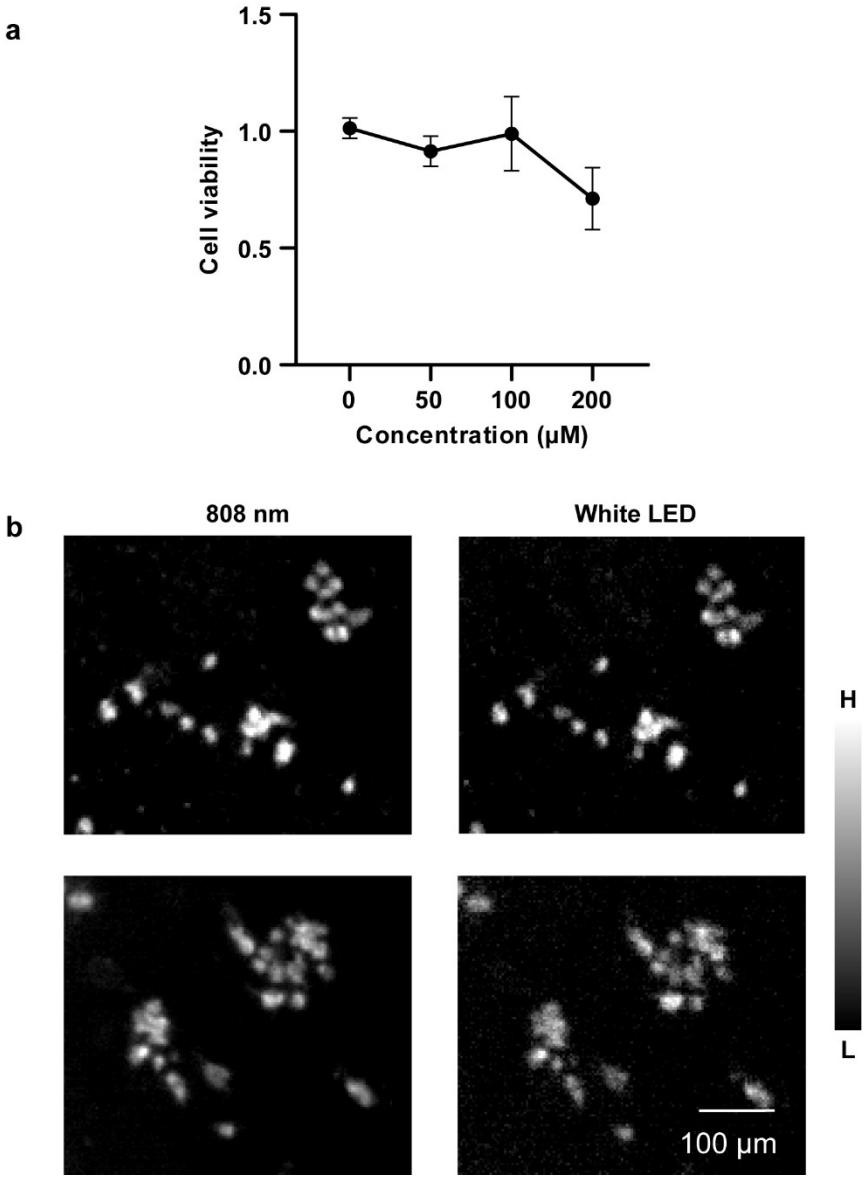

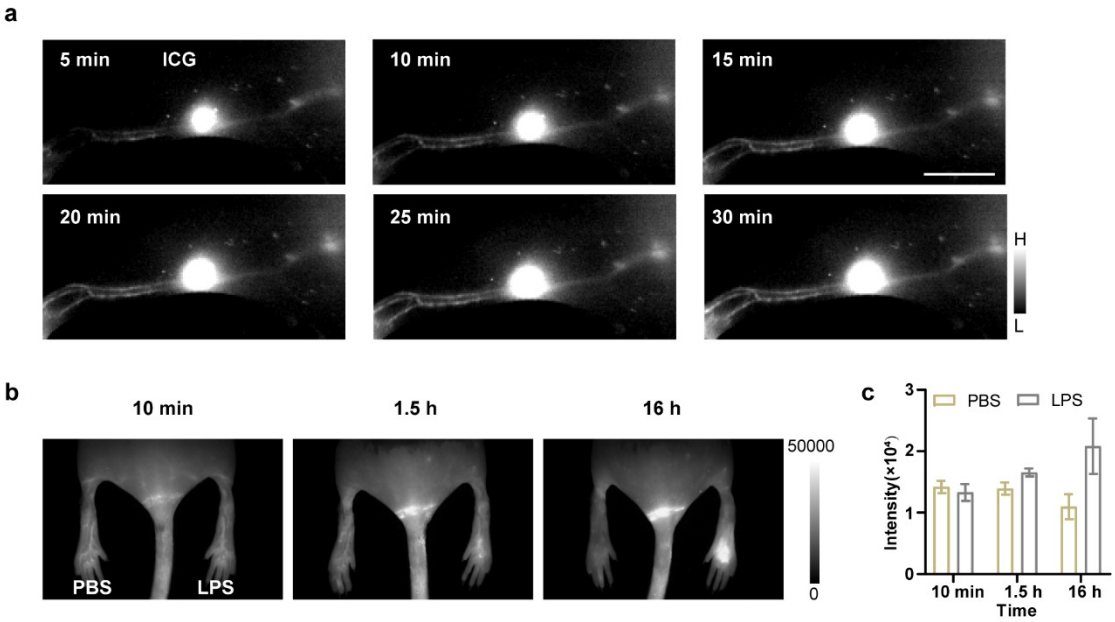

Supplementary Figure 8. a) Multi-wavelength LED excited NIR-II lymphatic imaging at different time points on normal Balb/c mice after injection of indocyanine green (ICG, 24 μg) (X-cite® 110LED, 1000 nm LP, 500 ms). Scale bar, 0.5 cm. b) NIR-II fluorescence imaging of LPS-treated and normal mice at different times after intravenous injection of TPA-TQT@BSA-H (200 μg, X-cite® 110LED, 1000 nm LP, 300 ms). c) Fluorescence intensity profiles of mouse foot pads in LPS-treated and normal groups over time.

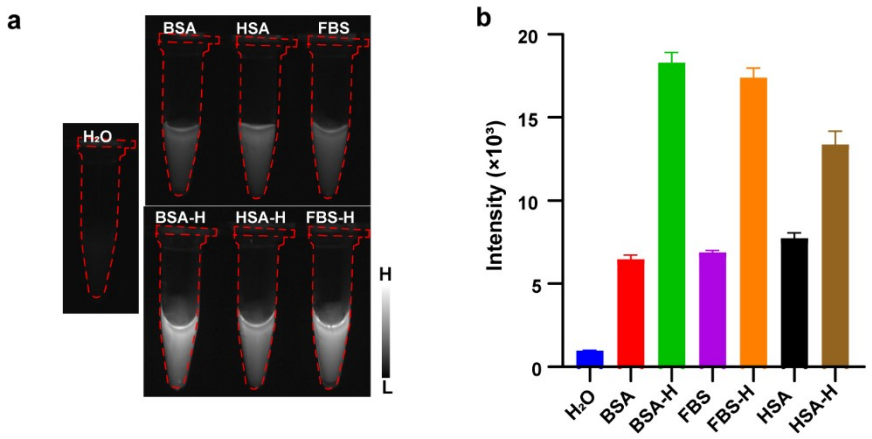

Supplementary Figure 9. **a)** X-Cite® 110LED induced NIR-II imaging of TPA-TQT in different media including H_2O, BSA, HSA, and FBS solution. (X-cite® 110LED, 1000 nm LP, 100 ms, 45 mW cm^{-2}). **b)** In **a**, the fluorescence intensities of TPA-TQT in different media were recorded.

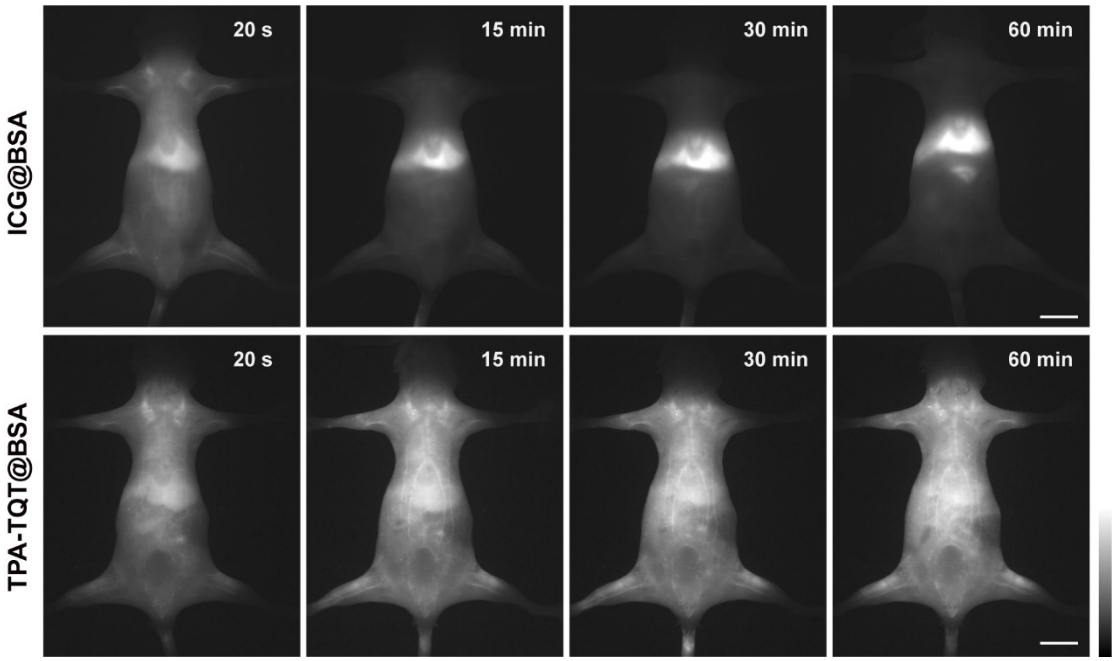

Supplementary Figure 10. Whole-body NIR-II imaging of normal balb/c mice with ICG@BSA-H complexes (65 nM, 1000 nm LP, 100 ms) and TPA-TQT@BSA-H complexes (65 nM, 1000 nm LP, 200 ms) excited by X-cite® 110LED. Scale bar: 1 cm.

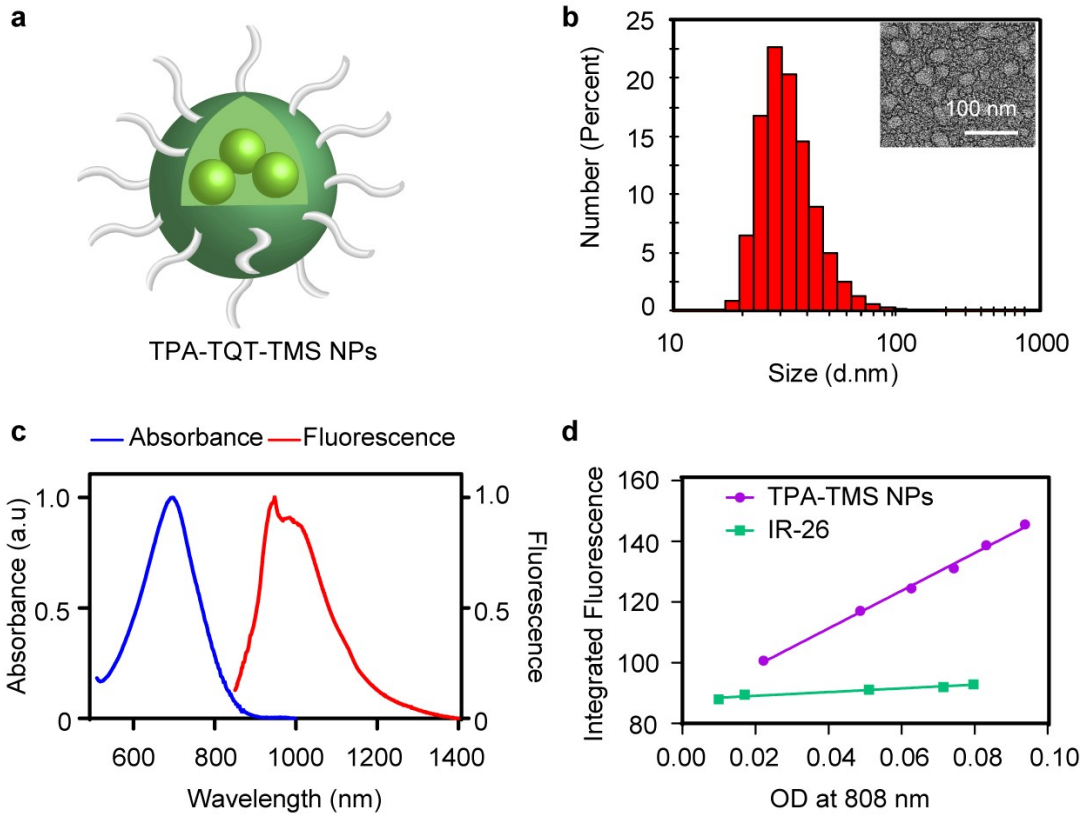

Supplementary Figure 11. **a**) Schematic illustration of TPA-TQT-TMS NPs. **b**) The dynamic light scattering (DLS) and transmission electron microscopy (TEM) images of TPA-TQT-TMS NPs. **c**) The absorption spectra and fluorescence spectra of TPA-TQT-TMS NPs in water. **d**) Plot of the integrated fluorescence spectrum of TPA-TQT-TMS NPs at different concentrations in deionized water. Linear fits were used to calculate quantum yield by comparing the slopes to reference IR-26 (QY = 0.05% in dichloroethane)

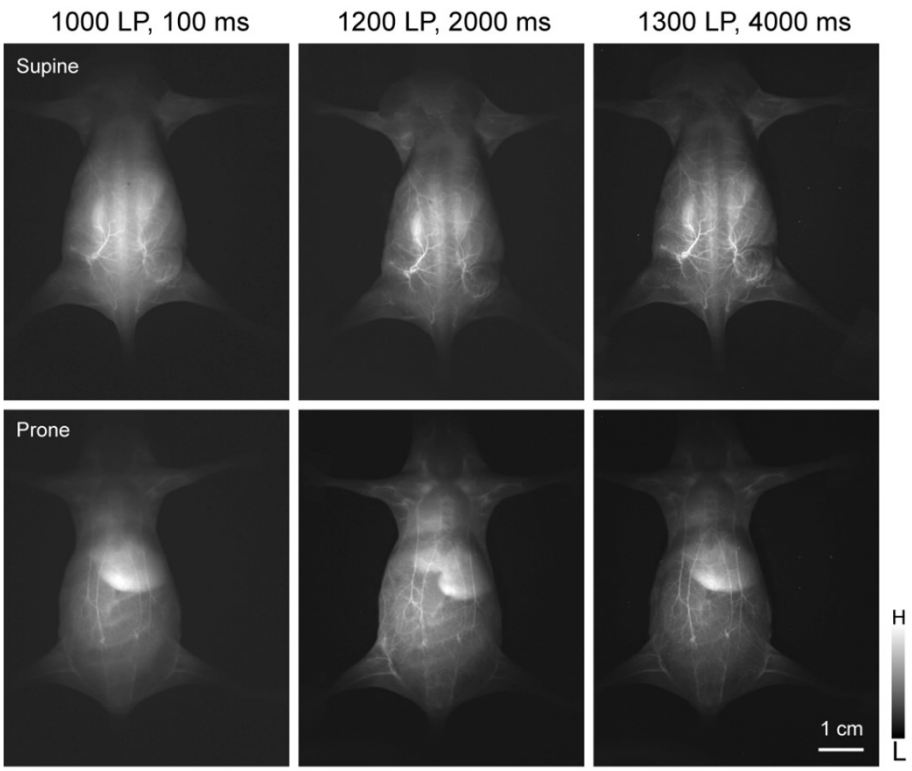

Supplementary Figure 12. Multi-wavelength (X-cite® 110LED) LED-excited NIR-II whole-body vessel imaging of U87MG tumor-bearing mice after TPA-TQT-TMS NPs (366 μg, 200 μL) administration. Scale bar: 1 cm.

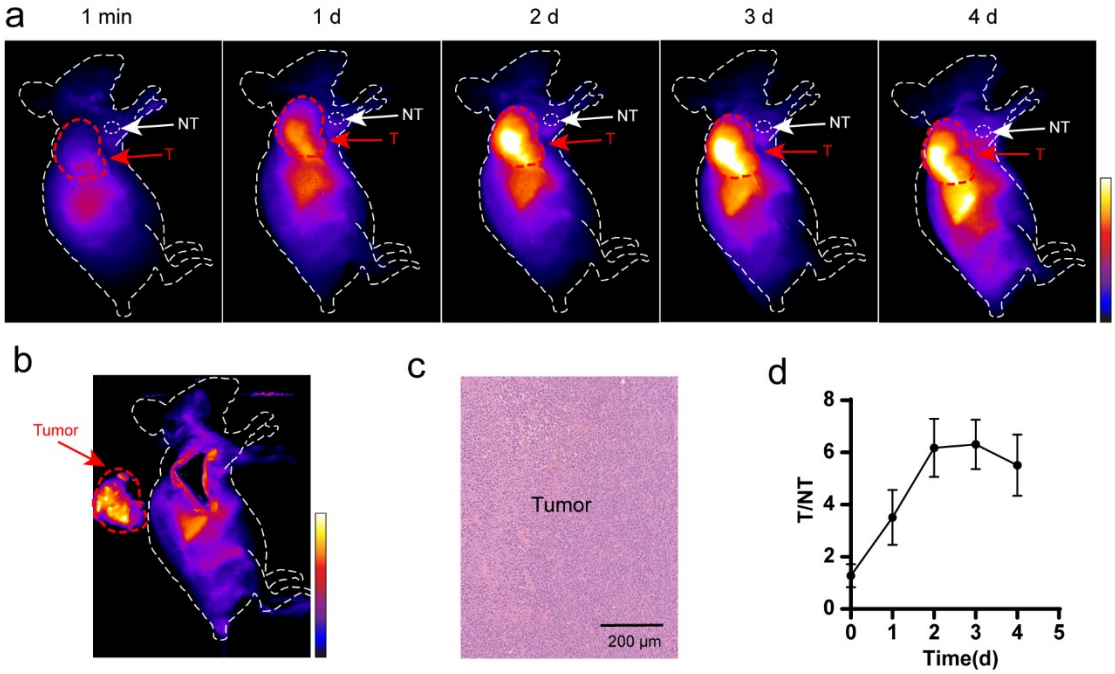

Supplementary Figure 13. Multi-wavelength (X-cite® 110LED) LED-based NIR-II imaging of subcutaneous 4T1 tumor-bearing mice. **a)** NIR-II imaging of 4T1 tumor-bearing mice at different time points after injection of TPA-TQT-TMS NPs (183 μg, 1000 nm LP, 100 ms). **b)** NIR-II image after subcutaneous 4T1 tumor dissection. **c)** H&E staining of the tumor. Scale bar: 200 μm. **d)** Tumor (red dotted circle) to normal tissue (white dotted circle) ratios (T/NT) at different time points.

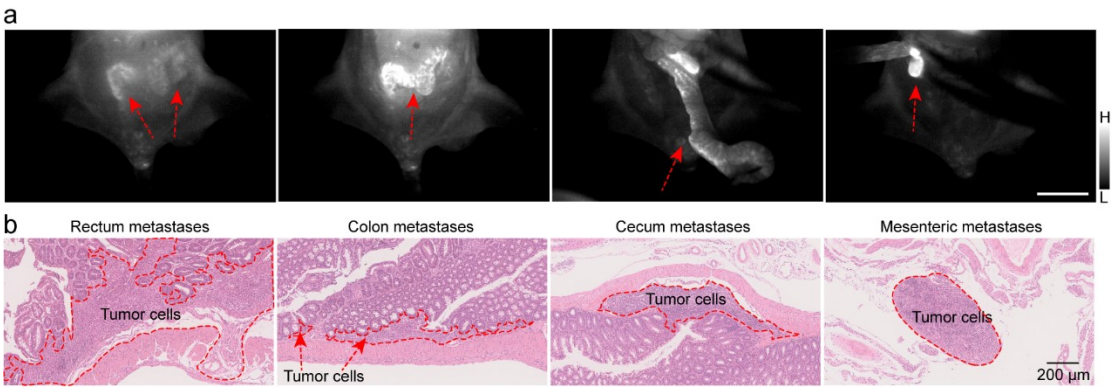

Supplementary Figure 14. Multi-wavelength LED-based NIR-II imaging of abdominal intestinal metastases in subcutaneous 4T1 tumor-bearing mice at 160 h after TPA-TQT-TMS NPs administration. **a)** NIR-II imaging of intestinal metastases (X-cite® 110 LED, 1000 nm LP, 1000 ms, 45 mW cm^{-2}). Scale bar, 1 cm. **b)** H&E staining of intestinal tumors. Scale bar, 200 μm. The red arrow indicates the tumor.

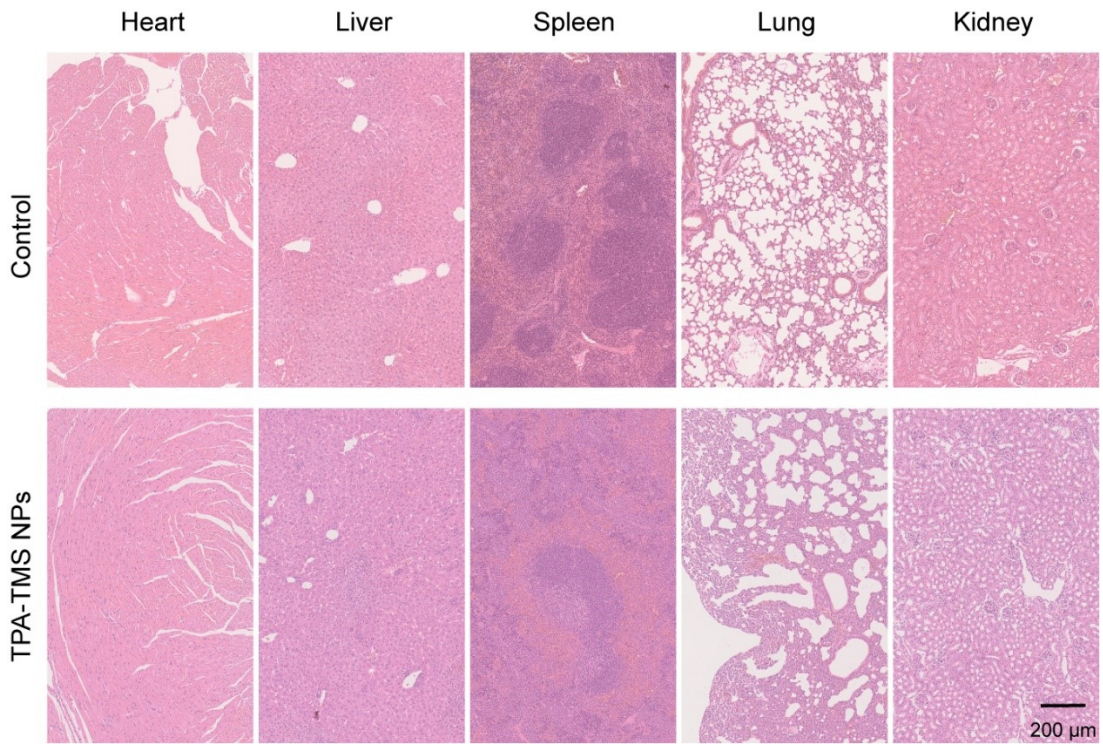

Supplementary Figure 15. Biocompatibility evaluation. Representative major organ histology (H&E stained) of mice in the control group and TPA-TQT-TMS NPs (183 μg) treated mice at 4 days post-injection. Scale bar: 200 μm.

Supplementary Table 1. Details of imaging parameters used in each fluorescent image of this study.

Figures	Dyes	Dose	Light source (nm/mWcm^{-2})	Filter sets (nm LP)	Exposure time (ms)
Fig. 1e	TPA-TQT	1, 5 μg/μL	X-Cite® 110 (LED)/45	1100 1200 1300	100
Fig. S3	TPA-TQT	Variou sconc.	LED room light/0.35	1000	1000
Fig. S9	TPA-TQT	Same conc.	X-Cite® 110 (LED)/45	1000	100
Fig. 1g,	TPA-TQT /ICG	-----	808/45 808/145 X-Cite® 110 (LED)/45	1000 1000 1000	10 100 200
Fig. S5	TPA-TQT	5 μg/μL	iPhone 12 X-Cite® 110 5.11 XBTA6 HUAWEI 50	1000	200
Fig. 2d	TPA-TQT	Variou sconc.	X-Cite® 110/40 Green LED/40 630 nm LED/40 660 nm LED/40 730 nm LED/40	1000	100
Fig. 2g	TPA-TQT	32 μg	X-Cite® 110/35 Green LED/35 630 nm LED/35 660 nm LED/35 730 nm LED/35	1000	100
Fig. 3b	TPA-TQT @ BSA-H	-----	X-Cite® 110 (LED)/45	1000	500
Fig. S6	TPA-TQT	-----	X-Cite® 110 (LED)/45	1000	200/500
Fig. S7b	TPA-TQT	100 μM	808 nm/140 X-Cite® 110 (LED)/45	1000	2000/5000

Fig. 3d, 3e	TPA-TQT@ BSA-H	50 μg	X-Cite® 110 (LED)/45	1100	200
Fig. 3f	TPA-TQT @BSA-H	50 μg	X-Cite® 110 (LED)/45	1000	500
Fig. S8a	ICG	24 μg	X-Cite® 110 (LED)/45	1000	500
Fig. S8b	TPA-TQT @BSA-H	200 μg		1000	300
Fig. 4a	ICG@BSA-H	65 nM	X-Cite® 110 (LED)/45	1000	300
Fig. 4a	TPA-TQT @ BSA-H	65 nM	X-Cite® 110 (LED)/45		400
			660 nm laser/48	1000	200
			808 nm laser/113		400
Fig. 4b	TPA-TQT @ BSA-H	65 nM	X-Cite® 110 (LED)/45	1000	200
				1100	500
				1200	5000
				1300	10000
Fig. 4c	TPA-TQT @ BSA-H	65 nM	X-Cite® 110 (LED)/45	1000	500
				1100	1000
				1200	2000
				1300	3000
Fig. S10	ICG@BSA	65 nM	X-Cite® 110 (LED)/45	1000	100
	TPA-TQT @ BSA-H	65 nM			200
Fig. 5b	TPA-TQT @ BSA-H	100 μg	X-Cite® 110 (LED)/45	1000	500
Fig. 6b	TPA-TQT-TMS NPs	366 μg	X-Cite® 110 (LED)/45	1000	300
				1200	2000
				1300	4000
Fig. 6d, S13	TPA-TQT-TMS NPs	183 μg	X-Cite® 110 (LED)/45	1000	100
Fig. 6f	TPA-TQT-TMS NPs	183 μg	Lighting LED	1000	1000

Fig. S12	TPA-TQT-TMS NPs	366 μg	X-Cite® 110 (LED)/45	1000 1200 1300	100 2000 4000
Fig. S14	TPA-TQT-TMS NPs	183 μg	X-Cite® 110 (LED)/45	1000	1000

Additional information

Supplementary Movie 1. X-cite®100 LED-excited NIR-II imaging of the hindlimb ischemia-reperfusion in mice (1000 LP, 500 ms, 45 $mW \cdot cm^{-2}$).

Supplementary Movie 2. NIR-II imaging guided 4T1 subcutaneous tumor surgery excited by lighting LED (1000 LP, 2000 ms, 45 $mW \cdot cm^{-2}$).

Supplementary Movie 3. NIR-II imaging guided liver metastasis resection excited by lighting LED (1000 LP, 2000 ms, 45 $mW \cdot cm^{-2}$).